Inorganic Chemistry
Article

Inorg. Chem. 2010, 49, 7935–7940 7935
DOI: 10.1021/ic100940b

# $BaGa_2Pn_2$ (*Pn* = P, As): New Semiconducting Phosphides and Arsenides with Layered Structures

**Hua He,[†] Ryan Stearrett,[‡] Edmund R. Nowak,[‡] and Svilen Bobev*[,†]**

[†]*Department of Chemistry and Biochemistry and* [‡]*Department of Physics and Astronomy, University of Delaware, Newark, Delaware 19716*

Received May 11, 2010

Reported are the synthesis, the structural characterization, and the electronic band structures of two new Zintl phases: $BaGa_2P_2$ and $BaGa_2As_2$. Both compounds are isoelectronic and isotypic and crystallize in a monoclinic system with a new structure type (Pearson symbol *mP*20). The structures have been established by single-crystal X-ray diffraction, space group $P2_1/c$ ($Z = 4$), with lattice parameters as follows: $a = 7.3363(13)/7.495(5)$ Å; $b = 9.6648(17)/9.901(6)$ Å; $c = 7.4261(13)/7.643(5)$ Å; $\beta = 115.373(2)°/115.381(8)°$ for $BaGa_2P_2/BaGa_2As_2$, respectively. The atomic arrangements in both cases are devoid of disorder and are best rationalized as polyanionic layers, $^2_\infty[Ga_2Pn_2]^{2-}$ (*Pn* = P, As), with $Ba^{2+}$ cations separating them. The layers, in turn, can be viewed as the result of condensation of $Ga_2Pn_6$ units, which are isosteric with the ethane molecule in its staggered conformation. Structural parallels with other known Zintl phases are presented. The electronic structures, computed using the tight-binding linear muffin-tin orbital methods (TB-LMTO), are discussed as well.

## Introduction

In recent years, there have been numerous reports on new ternary pnictides in the systems *A*-Tr-*Pn*, where *A* = Ca, Sr, Ba, Eu, Yb; Tr = Al, Ga, In; and *Pn* = P, As. Examples include $BaGa_2Sb_2$,[1] $Yb_5Al_2Sb_6$,[2] $Yb_5In_2Sb_6$,[3] $Ba_2In_5As_5$,[4] $Eu_3In_2P_4$,[5] $EuIn_2P_2$,[6] $EuGa_2As_2$,[7] $BaIn_2P_2$,[8] $Eu_3InP_3$,[9] $Ba_4In_8Sb_{16}$,[10] and $Ba_3Ga_4Sb_5$,[11] among others. Since there are significant differences in the electronegativities of the constituent elements, almost exclusively, the structures of such compounds obey the simple (octet) rules for electron counting in main-group chemistry. Therefore, in spite of the unusual and often complicated bonding patterns, the formulas of the above-named solids can be effectively rationalized if one assumes electron transfer from the cations to the anions, so that each element achieves a closed-shell configuration, that is, they can be classified as Zintl phases.[12] This renewed interest in such materials comes many years after the pioneering work of von Schnering, Schäfer, Eisenmann and Cordier,[13] and is largely due to the growing attention in thermoelectric energy technologies,[14] and the promise of such small-gap semiconductors with complex structures for use in energy-related applications.[15]

The past research efforts in our group have been closely aligned with studies on the crystal and electronic structures of new Zintl phases, both from a fundamental and practical standpoint. As a result of our previous activity in this field, we have already reported on a number of novel ternary pnictides whose bonding characteristics could be advantageous in the efforts to optimize the thermoelectric efficiency.[16] Most of the earlier work has been focused on antimonides and bismuthides with the $d^5$- and $d^{10}$-metals,[17] although we have also reported on several

*To whom correspondence should be addressed. E-mail: bobev@udel.edu. Phone: (302) 831-8720. Fax: (302) 831-6335.

(1) Kim, S. J.; Kanatzidis, M. G. *Inorg. Chem.* **2001**, *40*, 3781–3785.
(2) Todorov, I.; Chung, D. Y.; Ye, L.; Freeman, A. J.; Kanatzidis, M. G. *Inorg. Chem.* **2009**, *48*, 4768–4776.
(3) Kim, S. J.; Ireland, J. R.; Kannewurf, C. R.; Kanatzidis, M. G. *J. Solid State Chem.* **2000**, *155*, 55–61.
(4) Mathieu, J.; Achey, R.; Park, J. H.; Purcell, K. M.; Tozer, S. W.; Latturner, S. E. *Chem. Mater.* **2008**, *20*, 5675–5681.
(5) Jiang, J.; Olmstead, M. M.; Kauzlarich, S. M.; Lee, H. O.; Klavins, P.; Fisk, Z. *Inorg. Chem.* **2005**, *44*, 5322–5327.
(6) Jiang, J.; Kauzlarich, S. M. *Chem. Mater.* **2006**, *18*, 435–441.
(7) Goforth, A. M.; Hope, H.; Condron, C. L.; Kauzlarich, S. M.; Jensen, N.; Klavins, P.; MaQuilon, S.; Fisk, Z. *Chem. Mater.* **2009**, *21*, 4480–4489.
(8) Rauscher, J. F.; Condron, C. L.; Beault, T.; Kauzlarich, S. M.; Jensen, N.; Klavins, P.; MaQuilon, S.; Fisk, Z.; Olmstead, M. M. *Acta Crystallogr.* **2009**, *C65*, i69–i73.
(9) Jiang, J.; Payne, A. C.; Olmstead, M. M.; Lee, H. O.; Klavins, P.; Fisk, Z.; Kauzlarich, S. M.; Hermann, R. P.; Grandjean, F.; Long, G. J. *Inorg. Chem.* **2005**, *44*, 2189–2197.
(10) Kim, S. J.; Hu, S. Q.; Uher, C.; Kanatzidis, M. G. *Chem. Mater.* **1999**, *11*, 3154–3159.
(11) Park, S. M.; Kim, S. J.; Kanatzidis, M. G. *J. Solid State Chem.* **2003**, *175*, 310–315.
(12) (a) Kauzlarich, S. M., Ed.; *Chemistry, Structure, and Bonding of Zintl Phases and Ions*; VCH Publishers: New York, 1996. (b) Nesper, R. *Prog. Solid State Chem.* **1990**, *20*, 1–45. (c) Schäfer, H.; Eisenmann, B.; Müller, W. *Angew. Chem., Int. Ed. Engl.* **1973**, *12*, 694–712.
(13) von Schnering, H.-G. *Angew. Chem., Int. Ed. Engl.* **1981**, *20*, 33–51.
(14) (a) Snyder, G. J.; Toberer, E. S. *Nat. Mater.* **2008**, *7*, 105–114. (b) Kleinke, H. *Chem. Mater.* **2010**, *22*, 604–611.
(15) Kauzlarich, S. M.; Brown, S. R.; Snyder, G. J. *Dalton Trans.* **2007**, 2099–2107.
(16) Toberer, E. S.; May, A. F.; Snyder, G. J. *Chem. Mater.* **2010**, *22*, 624–634.
(17) (a) Saparov, B.; Xia, S.-Q.; Bobev, S. *Inorg. Chem.* **2008**, *47*, 11237–11244. (b) Xia, S.-Q.; Bobev, S. *J. Am. Chem. Soc.* **2007**, *129*, 4049–4057. (c) Xia, S.-Q.; Bobev, S. *J. Comput. Chem.* **2008**, *29*, 2125–2133. (d) Xia, S.-Q.; Bobev, S. *Inorg. Chem.* **2008**, *47*, 1919–1921.


Published on Web 08/11/2010

phases with main group polyanionic substructures: $Yb_{11}GaSb_9$,[18] $Sr_{11}InSb_9$,[19] $Eu_{11}InSb_9$ and $Yb_{11}InSb_9$,[20] $A_7Ga_2Sb_6$,[21] and $A_7Ga_8Sb_8$ and $Ba_7In_8Sb_8$.[22] Extending our research into the phosphides and arsenides, we first undertook systematic synthetic explorations in the Ba−Ga−P and Ba−Ga−As ternary systems. Herein we report the synthesis and the crystal structures of two new Zintl phases $BaGa_2P_2$ and $BaGa_2As_2$, whose novel structures feature $^2_\infty[Ga_2Pn_2]^{2-}$ ($Pn$ = P, As) layers with complex topology. $BaGa_2P_2$ is the second structurally characterized Ba−Ga−P compound, after $Ba_6Ga_2P_6$,[23] while $BaGa_2As_2$ is the first ever compound involving these three elements, suggesting that the respective ternary phase diagrams are insufficiently mapped out. Discussed as well are their electronic band structures, calculated using the tight-binding linear muffin-tin orbital (TB-LMTO) method.[24]

## Experimental Section

**Synthesis.** All manipulations involving elemental Ba were performed inside an argon-filled glovebox or under vacuum. The elements with stated purity greater than 99.9% were purchased from Alfa or Aldrich and used as received. Two general synthetic methods were explored: on-stoichiometry reactions in sealed niobium tubes, and flux reactions in alumina crucibles using gallium as reactive flux. Nb tubes were welded with an arc-welder under a partial pressure of high-purity argon gas. Before the heat-treatment in programmable tube or muffle furnaces, both the niobium tubes and the crucibles were enclosed in fused silica tubes, which were subsequently flame-sealed under vacuum (below discharge). Specific temperature profiles and other details are described in the Supporting Information section.

Crystals of $BaGa_2As_2$ were first identified as one of the products of a reaction loaded in the molar ratio Ba/Ga/As = 1:12:3. The large excess of Ga was intended as a flux. After the structure and the composition were established via X-ray diffraction, the synthesis was repeated with the correct stoichiometric ratio of Ba and As, and a 5-fold excess of Ga, that is, Ba/Ga/As = 1:10:2. The isostructural $BaGa_2P_2$ was synthesized from Ga flux reaction, setup in the same way. Such syntheses resulted in black, small grains, essentially pure $BaGa_2Pn_2$ ($Pn$ = P, As) phases (based on PXRD). Under a microscope, however, a very small amount of Ga was also noticed as tiny silvery droplets adhered to some of the crystals' surfaces. This hampered the property measurements and precluded the validation of the theoretically predicted small-gap semiconducting behavior (vide infra).

Subsequent experiments aimed at the growth of larger crystals were carried in the following ways: (1) at the same reaction temperature and with the same ratio of the elements, but with a slower cooling rate (−3 °C/h); (2) at the same reaction temperature and with the same cooling rates (both −3 °C/h and −6 °C/h), but with a different amounts of Ga. Neither scheme produced the desired large crystals of $BaGa_2Pn_2$.

We also note here that stoichiometric reactions of Ba, Ga, and P or As in welded Nb-tubes failed to produce the title compounds in high yields. The major products from such experiments were $Ba_7Ga_4As_9$[25] ($Ba_7Ga_4Sb_9$ type[26]), $Ba_3P_2$,[27] $BaGa_4$,[28] GaP, and GaAs.[29] Traces of NbAs and NbP[29] were also detected, indicating unwanted side reactions of As and P with the containers at elevated temperature. These observations indicate that stoichiometric reactions in sealed Nb-tubes are not well-suited for the synthesis of such materials; more expensive Ta- or Mo-tubes might be necessary. Also, from the results of synthetic experiments involving isothermal step at 500 °C, together with the fact that flux-grown $BaGa_2Pn_2$ ($Pn$ = P, As) crystals decompose upon heating (under vacuum or in atmosphere of Ar), we can speculate that the title compounds are metastable (kinetic) phases, "trapped" via the use of the flux-method. Both points above illustrate some of the difficulties for the exploration of the respective ternary systems, which could explain the scarce structural information in the Pearson's Handbook,[29] and the Inorganic Crystal Structure Database (ICSD),[30] where aside from $Ba_6Ga_2P_6$,[23] there are no other known examples with these elements.

Attempts to synthesize other isotypic compounds with the heavier pnicogens Sb and Bi and/or the lighter alkaline-earth metals Ca and Sr, or with the rare-earth metals Eu and Yb were unsuccessful. All reactions of Ba and Ga with Sb or Bi produced $BaGa_2Sb_2$,[1] $Ba_7Ga_4Sb_9$,[26] $BaGa_4$,[28] and $BaBi_2$,[31] as major phases. The outcome of the experiments with Ca, Sr, Eu, and Yb were mostly simple binary phases or known ternary compounds, except for the new compounds of $CaGa_2P_2$ ($EuIn_2P_2$ type[6]), $SrGa_2As_2$ ($EuGa_2As_2$ type[7]), and $CaGa_2As_2$ (own type, can be seen as a derivative structure of $EuIn_2P_2$).[32] Further details concerning the synthesis are provided in the Supporting Information section.

**Powder X-ray Diffraction (PXRD).** X-ray powder diffraction patterns were taken at room temperature on a Rigaku MiniFlex powder diffractometer, employing filtered Cu Kα radiation. The diffractograms were collected in the $2\theta$ range from 10° to 75°. Data analysis was done using software from MDI-JADE. The positions of the peaks and their intensities matched very well with the calculated patterns from the refined structure. Since the diffractometer was enclosed and operated in a nitrogen-filled glovebox, the air-sensitivity of the title compounds could be tested by comparing the diffraction patterns of freshly prepared samples with those that had been exposed to air. According to this, polycrystalline specimens of $BaGa_2As_2$ and $BaGa_2P_2$ are stable for up to 2 weeks.

**Single-Crystal X-ray Diffraction.** X-ray single-crystal diffraction data were collected on a Bruker SMART CCD-based diffractometer, employing monochromated Mo $K\alpha_1$ radiation. Crystals from freshly prepared samples were inspected under a microscope and cut to less than 100 $\mu$m in all dimensions. Then, the crystals were mounted on glass fibers using Paratone-N oil, which hardens at low temperature maintained by a cold nitrogen stream (200(2) K). After ensuring the crystal quality, full spheres of data were collected in four batch runs with frame width of 0.4° for $\omega$ and $\theta$. Exposure time varied between 8 and 14 s/frame, depending on the size and quality of that crystal. Data collection and data integration were done using SMART[33] and SAINTplus

(18) Bobev, S.; Fritsch, V.; Thompson, J. D.; Sarrao, J. L.; Eck, B.; Dronskowski, R.; Kauzlarich, S. M. *J. Solid State Chem.* **2005**, *178*, 1071–1079.
(19) Hullmann, J.; Xia, S.-Q.; Bobev, S. *Acta Crystallogr., Sect. E* **2007**, *63*, i178.
(20) Xia, S.-Q.; Hullmann, J.; Bobev, S.; Ozbay, A.; Nowak, E. R.; Fritsch, V. *J. Solid State Chem.* **2007**, *180*, 2088–2094.
(21) Xia, S.-Q.; Hullmann, J.; Bobev, S. *J. Solid State Chem.* **2008**, *181*, 1909–1914.
(22) Bobev, S.; Hullmann, J.; Harmening, T.; Pöttgen, R. *Dalton Trans.* **2010**, *39*, 6049−6055.
(23) Peters, K.; Carrillo-Cabrera, W.; Somer, M.; von Schnering, H.-G. *Z. Kristallogr.* **1996**, *211*, 53–53.
(24) Skriver, H. L. *The LMTO Method*; Springer: Berlin, 1984.
(25) He, H.; Bobev, S. unpublished results: $Ba_7Ga_4As_9$ in *Pmmn* ($Ba_7Ga_4Sb_9$ type[26]), $a$ = 10.184(2) Å; $b$ = 16.987(4) Å; $c$ = 6.8012(14) Å.
(26) (a) Cordier, G.; Schäfer, H.; Stelter, M. *Z. Anorg. Allg. Chem.* **1986**, *534*, 137–142. (b) Alemany, P.; Alvarez, S.; Hoffmann, R. *Inorg. Chem.* **1990**, *29*, 3070–3073.
(27) Maass, K.-E. *Naturwissenschaften* **1968**, *55*, 489–490.
(28) Bruzzone, G. *Acta Crystallogr.* **1965**, *18*, 1081–1082.
(29) (a) Villars, P.; Calvert, L. D., Ed.; *Pearson's Handbook of Crystallographic Data for Intermetallic Phases*, 2nd ed.; ASM International: Materials Park, OH, 1991. (b) Villars, P. *Pearson's Handbook of Crystallographic Data for Intermetallic Phases*, desktop ed.; ASM International: Materials Park, OH, 1997.
(30) *ICSD Database*; Fachinformationszentrum: Karlsruhe, Germany, 2009.
(31) He, H.; Bobev, S. unpublished results: $BaBi_2$ in $I4_1/amd$ ($HfGa_2$ type[29]), $a$ = 4.939(4) Å; $c$ = 36.38(2) Å.
(32) He, H.; Bobev, S. unpublished results: $CaGa_2As_2$ in $R\bar{3}m$ (own type), $a$ = 3.9904(5) Å; $c$ = 24.821(4) Å.
(33) *SMART NT*, Version 5.63; Bruker Analytical X-ray Systems, Inc.: Madison, WI, 2003.

**Table 1.** Selected Crystal Data and Structure Refinement Parameters for $BaGa_2P_2$ and $BaGa_2As_2$

| | $BaGa_2P_2$ | $BaGa_2As_2$ |
|---|---|---|
| fw, $g \cdot mol^{-1}$ | 338.72 | 426.62 |
| crystal system | monoclinic | |
| space group | $P2_1/c$ (No. 14), $Z = 4$ | |
| $\lambda$, Å | 0.71073 | |
| $T$, K | 200(2) | |
| $a$, Å | 7.3363(13) | 7.495(5) |
| $b$, Å | 9.6648(17) | 9.901(6) |
| $c$, Å | 7.4261(13) | 7.643(5) |
| $\beta$, deg | 115.373(2) | 115.381(8) |
| $V$, Å$^3$ | 475.8(2) | 512.5(6) |
| $\rho_{calcd}$, $g \cdot cm^{-3}$ | 4.729 | 5.530 |
| $\mu$ (Mo K$\alpha$), $cm^{-1}$ | 199.01 | 306.68 |
| GOF on $F^2$ | 1.016 | 0.982 |
| $R_1$ $[I > 2\sigma(I)]^a$ | 0.0188 | 0.0230 |
| $wR_2$ $[I > 2\sigma(I)]^a$ | 0.0386 | 0.0401 |
| largest peak/hole ($e^- \cdot$ Å$^{-3}$) | 1.150/−0.604 | 1.056/−1.084 |

[a] $R_1 = \sum||F_o| - |F_c||/\sum|F_o|$; $wR_2 = [\sum w(F_o^2 - F_c^2)^2/\sum w(F_o^2)^2]^{1/2}$, and $w = 1/[\sigma^2 F_o^2 + (AP)^2]$, $P = (F_o^2 + 2F_c^2)/3$; $A$ is a weight coefficient, refined as follows: $A = 0.0189$ for $BaGa_2P_2$, $A = 0.0148$ for $BaGa_2As_2$.

**Table 2.** Atomic Coordinates and Equivalent Isotropic Displacement Parameters ($U_{eq}$[a]) for $BaGa_2P_2$ and $BaGa_2As_2$

| atom | Wyckoff Site | $x$ | $y$ | $z$ | $U_{eq}$ (Å$^2$) |
|---|---|---|---|---|---|
| | | $BaGa_2P_2$ | | | |
| Ba | 4*e* | 0.41793(3) | 0.39896(2) | 0.22493(3) | 0.0118(1) |
| Ga1 | 4*e* | 0.06058(6) | 0.71153(4) | 0.12614(6) | 0.0102(1) |
| Ga2 | 4*e* | 0.06032(6) | 0.01243(4) | 0.23816(6) | 0.0103(1) |
| P1 | 4*e* | 0.2062(1) | 0.1133(1) | 0.0318(1) | 0.0103(2) |
| P2 | 4*e* | 0.7365(2) | 0.3212(1) | 0.0540(1) | 0.0103(2) |
| | | $BaGa_2As_2$ | | | |
| Ba | 4*e* | 0.41449(5) | 0.39946(3) | 0.22044(4) | 0.0128(1) |
| Ga1 | 4*e* | 0.05604(8) | 0.71022(5) | 0.12969(8) | 0.0110(1) |
| Ga2 | 4*e* | 0.06196(8) | 0.01341(6) | 0.24053(8) | 0.0112(1) |
| As1 | 4*e* | 0.21283(8) | 0.11116(5) | 0.03135(8) | 0.0110(1) |
| As2 | 4*e* | 0.73302(8) | 0.31913(5) | 0.04844(8) | 0.0106(1) |

[a] $U_{eq}$ is defined as one-third of the trace of the orthogonalized $U_{ij}$ tensor.

software,[34] respectively. SADABS[35] was used for semiempirical absorption correction based on equivalent reflections. The structures were solved in the monoclinic space group $P2_1/c$ by direct methods, as implemented in the SHELXL-package.[36] The solutions provided the positions of all atoms in the asymmetric unit, and the subsequent refinements by full matrix least-squares on $F^2$ converged quickly to low residual factors and flat difference Fourier maps. Refining the atoms with anisotropic displacement parameters confirmed that the structure is devoid of disorder and all of the sites are fully occupied. In the last refinement cycles, the unit cell axes and the atomic coordinates were standardized with the aid of the Structure TIDY program.[37] Crystal data and details of the data collection are summarized in Table 1. Positional and equivalent isotropic displacement parameters and refined bond distances and angles are listed in Tables 2 and 3, respectively. Additional information on the crystal structure

**Table 3.** Important Interatomic Distances (Å) and Angles (deg) in $BaGa_2P_2$ and $BaGa_2As_2$

| $BaGa_2P_2$ | | $BaGa_2As_2$ | |
|---|---|---|---|
| Ga1−Ga2 | 2.5042(6) | Ga1−Ga2 | 2.513(1) |
| Ga1−P2 | 2.411(1) | Ga1−As2 | 2.506(1) |
| Ga1−P2 | 2.440(1) | Ga1−As2 | 2.526(1) |
| Ga1−P1 | 2.471(1) | Ga1−As1 | 2.565(1) |
| Ga2−Ga1 | 2.5042(6) | Ga2−Ga1 | 2.513(1) |
| Ga2−P1 | 2.419(1) | Ga2−As1 | 2.514(1) |
| Ga2−P1 | 2.441(1) | Ga2−As1 | 2.532(1) |
| Ga2−P2 | 2.459(1) | Ga2−As2 | 2.557(1) |
| P1−Ga2 | 2.419(1) | As1−Ga2 | 2.514(1) |
| P1−Ga2 | 2.441(1) | As1−Ga2 | 2.532(1) |
| P1−Ga1 | 2.471(1) | As1−Ga1 | 2.565(1) |
| P2−Ga1 | 2.411(1) | As2−Ga1 | 2.506(1) |
| P2−Ga1 | 2.440(1) | As2−Ga1 | 2.526(1) |
| P2−Ga2 | 2.459(1) | As2−Ga2 | 2.557(1) |
| P2−Ga1−Ga2 | 122.12(3) | As2−Ga1−Ga2 | 122.35(4) |
| P1−Ga1−Ga2 | 111.87(3) | As1−Ga1−Ga2 | 112.78(5) |
| P2−Ga1−Ga2 | 96.64(3) | As2−Ga1−Ga2 | 97.23(5) |
| P2−Ga1−P1 | 101.12(4) | As2−Ga1−As1 | 102.00(4) |
| P2−Ga1−P1 | 112.24(4) | As2−Ga1−As1 | 111.59(5) |
| P2−Ga1−P2 | 109.47(4) | As2−Ga1−As2 | 107.54(5) |
| P1−Ga2−Ga1 | 105.93(3) | As1−Ga2−Ga1 | 106.43(5) |
| P1−Ga2−Ga1 | 114.57(3) | As1−Ga2−Ga1 | 113.68(5) |
| P2−Ga2−Ga1 | 123.28(3) | As2−Ga2−Ga1 | 123.53(5) |
| P1−Ga2−P2 | 112.76(4) | As1−Ga2−As2 | 112.23(5) |
| P1−Ga2−P2 | 101.43(4) | As1−Ga2−As2 | 102.05(5) |

investigations, in the form of CIF files, can be obtained from the Supporting Information and from the Fachinformationszentrum Karlsruhe, 76344 Eggenstein-Leopoldshafen, Germany, (fax: (49) 7247−808−666; e-mail: crysdata@fiz.karlsruhe.de) with depository numbers: CSD-380479 for $BaGa_2P_2$ and CSD-380478 for $BaGa_2As_2$.

**Electronic Structure Calculations.** The Stuttgart TB-LMTO 4.7 program[38] was used to calculate band structures employing the tight-binding linear muffin-tin orbital (TB-LMTO) method.[24] Local density approximation (LDA) was used to treat exchange and correlation. All relativistic effects except for spin−orbital coupling were taken into account by the scalar relativistic approximation. The basis set included the 5d, 6s, and 6p orbitals for Ba, 4s, 4p, and 4d orbitals for Ga, 4s, 4p, and 4d orbitals for As, and 3s, 3p, and 3d orbitals for P. The 6p orbital of Ba, 4d orbital of Ga, 4d orbital of As, and 3d orbital of P were treated with the downfolding technique. The $k$-space integrations were performed by the tetrahedron method, using 650 irreducible $k$-points in the Brillouin zone. The total and partial density-of-states (DOS) were ploted and studied. To interrogate the chemical bonding, crystal orbital Hamilton populations (COHP)[39] of selected interactions were also analyzed. In the DOS and COHP plots, the Fermi level was set as a reference point at 0 eV.

**Property Measurements.** For both $BaGa_2P_2$ and $BaGa_2As_2$, direct current (dc) magnetization measurements and resistivity measurements were performed as a function of the temperature. In both cases, the lack of suitable single-crystals necessitated the use of polycrystalline samples, which inadvertently contained trace amounts of gallium (vide supra). The contactless magnetization (M) measurements were affected to a lesser degree by the free Ga and revealed temperature independent behavior, consistent with the closed-shell electronic configurations of the participating elements. However, the measurements of the electrical resistivity for different batches differed significantly, evidently because of different amounts of Ga in the samples. As a consequence, $\rho(T)$ dependence resembled the behavior of a poor metal, not of a semiconductor. The onset of the gallium superconducting transition below 5−6 K was also observed.

(34) *SAINT NT*, Version 6.45; Bruker Analytical X-ray Systems, Inc.: Madison, WI, 2003.
(35) *SADABS NT*, Version 2.10; Bruker Analytical X-ray Systems, Inc.: Madison, WI, 2001.
(36) *SHELXS-97*; Bruker Analytical Systems, Inc.: Madison, WI, 1990. (b) *SHELXTL*, Version 6.12; Bruker Analytical X-ray Systems, Inc.: Madison, WI, 2001.
(37) (a) Parthe, E.; Gelato, L. M. *Acta Crystallogr.* **1984**, *A40*, 169–183. (b) Gelato, L. M.; Parthe, E. *J. Appl. Crystallogr.* **1987**, *20*, 139–143.
(38) Jepsen, O.; Andersen, O. K. *TB-LMTO-ASAP program*, version 4.7; Max-Planck-Institut für Festkörperforschung: Stuttgart, Germany, 1998.
(39) Dronskowski, R.; Blöchl, P. *J. Phys. Chem.* **1993**, *97*, 8617–8624.

All attempts to remove the leftover gallium flux by treating the samples with iodine solution in dimethylformamide (DMF)[40] or with dilute hydrochloric acid failed. These traits, as well as details concerning the measurements with representative plots of $\chi_m(T)$ and $\rho(T)$ are provided in the Supporting Information section.

## Results and Discussion

**Crystal Structure.** Crystallographic data for the title compounds is summarized in Tables 1−3. Despite being "1-2-2" compounds, $BaGa_2P_2$ and $BaGa_2As_2$ are *not* isostructural to any of the common $AM_2X_2$ structure types: $CaAl_2Si_2$ (Pearson symbol *hP*5),[41] $ThCr_2Si_2$ (sometimes referred to as $CeAl_2Ga_2$; Pearson symbol *tI*10), and $CaBe_2Ge_2$ (Pearson symbol *tP*10).[42] Interestingly, the isoelectronic and closely related $BaGa_2Sb_2$ (Pearson symbol *oP*40),[1] $EuGa_2As_2$ (Pearson symbol *mP*20),[7] $BaIn_2P_2$ (Pearson symbol *mP*20),[8] and $EuIn_2As_2$ (Pearson symbol *hP*10),[43] are not isostructural to the title compounds either. Since these structural arrangements will be compared at length in the following discussion, for sake of clarity, schematic representations of all these structures are provided in the Supporting Information section. In the next paragraphs, the important characteristics of the structure will be briefly described, alongside a detailed examination of the chemical bonding, and a depiction of some useful structural relationships.

$BaGa_2Pn_2$ (*Pn* = P, As) crystallize in the monoclinic space group $P2_1/c$ (No. 14) with four formula units per cell. The exact same atomic arrangement is previously unknown, thereby constituting a new structure type with Pearson symbol *mP*20, adding to the diversity of the "1-2-2" compounds. This new structure contains five crystallographic distinct atoms in the asymmetric unit, one Ba, two Ga, and two pnicogens, all in general positions. Following the electronegativity differences among the constituting elements ($\chi_{Ba}$ = 0.9, $\chi_{Ga}$ = 1.6, $\chi_P$ = 2.1, and $\chi_{As}$ = 2.0),[44] the structure can be best described as polyanionic $^2_\infty[Ga_2Pn_2]^{2-}$ layers and $Ba^{2+}$ cations filling the space between them (Figure 1). The layers are well-separated from one another with closest contacts between adjacent *Pn*-vertices on the order of 4.3 Å (center-to-center separation can be approximated by the *a*-axis).

Within the anionic layers, Ga1 and Ga2 atoms are both found in tetrahedral coordination, each bonded to another Ga and to three pnicogen atoms in a staggered, ethane-like $[Pn_3Ga-GaPn_3]^{14-}$ conformation. The $[Ga_2Pn_6]^{14-}$ units are fused in two dimensions by sharing all of their pnicogen apexes, that is, $^2_\infty[Ga_2Pn_{6/3}]^{2-}$. Ga−Ga distances are virtually the same in both cases: 2.5042(6) Å in $BaGa_2P_2$ and 2.513(1) Å in $BaGa_2As_2$, respectively. Since the Ga−Ga bond length nearly equals twice the covalent radius of Ga ($r_{Ga}$ = 1.246 Å),[44] one can expect a typical 2-center 2-electron interaction. Indeed, an inspection of the Ga−Ga distances reported for other intermetallic compounds with similar bonding patterns reveals very comparable values: $d_{Ga-Ga}$ = 2.523 and 2.565 Å in $BaGa_2Sb_2$,[1] $d_{Ga-Ga}$ = 2.414, 2.459, and 2.473 Å in $EuGa_2As_2$,[7] $d_{Ga-Ga}$ = 2.481−2.585 Å in $A_7Ga_2Sb_6$,[21] and $d_{Ga-Ga}$ = 2.541 Å in $Na_2Ga_3Sb_3$.[45] The Ga−P and Ga−As distances are also within the norms (Table 3), with values that compare well with both the sums of the covalent radii ($r_P$ = 1.10 Å; $r_{As}$ = 1.21 Å),[44] and with the published literature: $d_{Ga-As}$ = 2.494−2.539 Å in $EuGa_2As_2$,[7] $d_{Ga-As}$ = 2.444−2.556 Å in $K_3Ga_3As_4$,[46] $d_{Ga-P}$ = 2.434−2.460 Å in $Ba_6Ga_2P_6$,[23] $d_{Ga-P}$ = 2.402−2.456 Å in $EuGa_2P_2$,[7], and so forth.

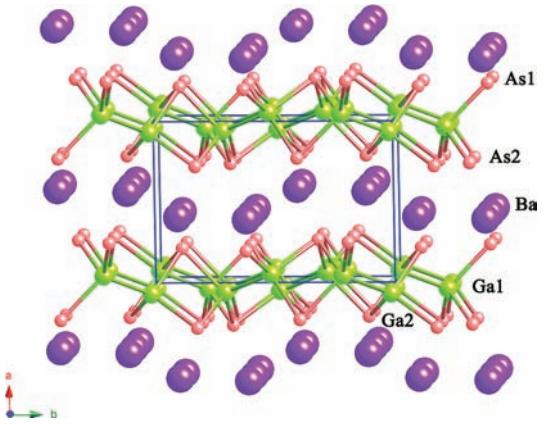


**Figure 1.** Perspective view of the structure of $BaGa_2As_2$, projected along the *c* axis. The Ba atoms are shown as purple spheres, the As atoms are shown as small red spheres, and the Ga atoms are drawn as green spheres. The unit cell is outlined.

Ba-coordination is distorted octahedral with "normal" Ba−P and Ba−As distances (Table 3). There are no close Ba−Ba interactions. Thus, taking into account the Ga−Ga single-bonds, the oxidation state of Ga should be assigned as +2, and the formulas can be rationalized as $(Ba^{2+})(Ga^{2+})_2(Pn^{3-})_2$, that is, Zintl phases.[12] Alternatively, the electron count can be approached from a standpoint of the formal charges, which gives the following breakdown: $(Ba^{2+})(4b\text{-}Ga^{1-})_2(3b\text{-}Pn^0)_2$, where the abbreviations 4*b*- and 3*b*- denote 4-bonded and 3-bonded atoms, respectively. Electronic band structure calculations, presented below, reveal a gap at the Fermi level, thereby confirming the closed-shell configuration of all atoms. However, unlike the description above, which is based on the classic Zintl formalism,[12] the *ab initio* results indicate a more complicated bonding picture, where Ba atoms are not fully ionized and should not be regarded as spacers/electron donors, and they participate in covalent interactions with the polyanionic network.

**Relationship to Other Structures.** The parallel between the $[Ga_2Pn_6]^{14-}$ building blocks of the polyanionic $^2_\infty[Ga_2Pn_2]^{2-}$ layers and the ethane molecule was already noted. Such anionic fragments are not unprecedented and appear to be a recurring motif in the crystal chemistry of many ternary pnictides and chalcogenides of the triel and tetrel elements. We can point out that staggered $[M_2X_6]$ fragments are also observed as isolated units, such as $[Sn_2P_6]^{12-}$ in $Ba_6Sn_2P_6$,[47] and $[Ga_2Sb_6]^{14-}$ in $A_7Ga_2Sb_6$.[21]

(40) Gray, D. L.; Francisco, M. C.; Kanatzidis, M. G. *Inorg. Chem.* **2008**, *47*, 7243–7248.
(41) (a) Zheng, C.; Hoffmann, R.; Nesper, R.; Vonschnering, H.-G. *J. Am. Chem. Soc.* **1986**, *108*, 1876–1884. (b) Zheng, C.; Hoffmann, R. *J. Phys. Chem.* **1985**, *89*, 4175–4181.
(42) (a) Burdett, J. K.; Miller, G. J. *Chem. Mater.* **1990**, *2*, 12. (b) Johrendt, D.; Felser, C.; Jepsen, O.; Andersen, O. K.; Mewis, A.; Rouxel, J. *J. Solid State Chem.* **1997**, *130*, 254–265.
(43) Goforth, A. M.; Klavins, P.; Fettinger, J. C.; Kauzlarich, S. M. *Inorg. Chem.* **2008**, *47*, 11048–11056.
(44) Pauling, L. *The Nature of the Chemical Bond*; Cornell University Press: Ithaca, NY, 1960.
(45) Cordier, G.; Ochmann, H.; Schäfer, H. *Mater. Res. Bull.* **1986**, *21*, 331–336.
(46) Birdwhistell, T. L. T.; Stevens, E. D.; O'Connor, C. J. *Inorg. Chem.* **1990**, *29*, 3892–3894.
(47) Eisenmann, B.; Jordan, H.; Schäfer, H. *Z. Naturforsch. B* **1983**, *38*, 404–406.

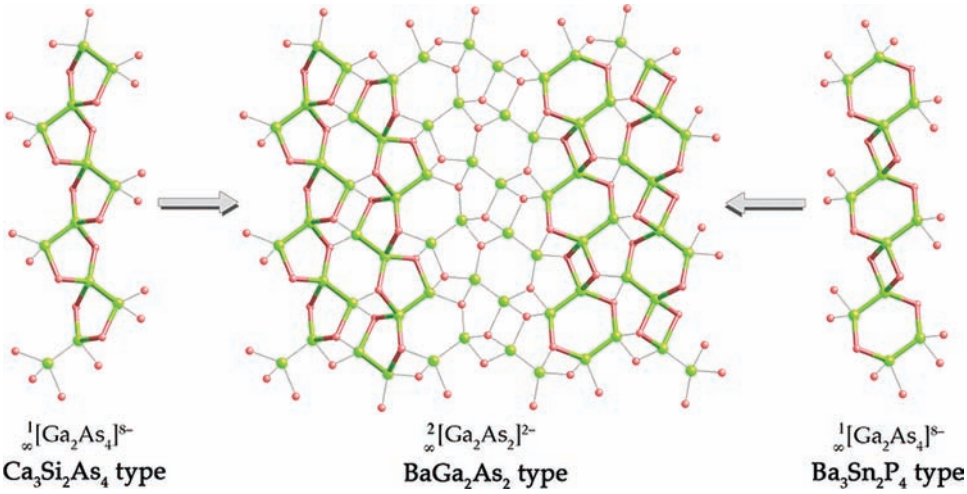


**Figure 2.** Schematic representation of the relationship between the $^2_\infty[Ga_2As_2]^{2-}$ layers in the structure of $BaGa_2As_2$ and the hypothetical $^1_\infty[Ga_2As_4]^{8-}$ chains, isosteric to $^1_\infty[Si_2As_4]^{6-}$ and $^1_\infty[Sn_2P_4]^{6-}$ known for the $Ca_3Si_2As_4$ (left) and the $Ba_3Sn_2P_4$ structure type (right), respectively. Color code as in Figure 1. Ba atoms are not shown for clarity. See the text for further details.

Condensation of $[Sn_2P_6]^{12-}$ and $[Si_2As_6]^{12-}$ moieties into $^1_\infty[Sn_2P_2P_{4/2}]^{6-}$ and $^1_\infty[Si_2As_2As_{4/2}]^{6-}$ one-dimensional (1D)-chains can be represented by the $Ba_3Sn_2P_4$[48] and $Ca_3Si_2As_4$ structures,[49] respectively. 2D-layers, as already mentioned are known for $EuGa_2Pn_2$,[7] $EuIn_2Pn_2$,[6,43] $BaIn_2P_2$,[8] $A_7Ga_8Pn_8$,[22] and the herein reported $BaGa_2Pn_2$ ($Pn$ = As, P). The $BaGa_2Sb_2$ structure[1] is a good example of a three-dimensional (3D) $^3_\infty[Ga_2Sb_2]^{2-}$ framework based on ethane-like $[Ga_2Sb_6]^{14-}$ units.

Closer examination of the $^2_\infty[Ga_2Pn_2]^{2-}$ layers in $BaGa_2Pn_2$ ($Pn$ = P, As) reveals four-, five-, and six-membered rings: the center pane of Figure 2 shows a top view of a layer, where these fragments are emphasized. The figure also highlights the structural resemblances between the $Ba_3Sn_2P_4$[48] and the $Ca_3Si_2As_4$[49] structure types (featuring $^1_\infty[Sn_2P_2P_{4/2}]^{6-}$ and $^1_\infty[Si_2As_2As_{4/2}]^{6-}$ chains) and the structures of the title compounds. The left diagram in Figure 2 depicts a hypothetical $^1_\infty[Ga_2As_4]^{8-}$ chain made up of five-membered rings and isosteric to $^1_\infty[Si_2As_4]^{6-}$, found in $Ca_3Si_2As_4$.[49] It is then clear that the layer under consideration can be viewed as an alternating array of such chains, where every other one is generated through inversion. Such "construction" requires sharing of all pnicogen vertices, concomitant to a 3-fold reduction of the formal charge, that is, $^2_\infty[Ga_2As_{6/2}]^{2-}$. The same cut-and-paste idea could also be used with different modular blocks, namely, the $^1_\infty[Ga_2As_4]^{8-}$ chains depicted to the right in Figure 2. The very same 1D-motif with characteristic four- and six-membered rings is present in the $Ba_3Sn_2P_4$ structure type.[48] Here, again, the condensation of a $^1_\infty[Ga_2As_4]^{8-}$ chain and its image from a glide operation through the "unshared" As atoms results in the formation of the $^2_\infty[Ga_2As_2]^{2-}$. Arguably, there will be many other ways to identify periodic building units, either 0D- or 1D-, which can be used to draw different structural parallels, for example, the topology of the layers could also be related to the $^1_\infty[Si_2As_4]^{6-}$ chains, known for the $Sr_3Si_2As_4$ structure type.[49] This analogy is schematically illustrated in the Supporting Information.

Alternatively, the structure of $BaGa_2Pn_2$ ($Pn$ = P, As), as well as those of $Ba_3Sn_2P_4$, $Ca_3Si_2As_4$, and $Sr_3Si_2As_4$ can be related to close-packed arrays of pnicogen atoms, with dimers of triel or tetrel atoms filling a certain fraction of the octahedral holes. This is easy to visualize since the $Ba^{2+}$ cations and the $[Ga_2]$ dumbbells are both found in distorted octahedra of pnicogen atoms (notice that dumbbells are aligned along one of the 3-fold axes, see Supporting Information). Hence, the overall structure could be viewed as *ccp* array of pnicogen atoms, with $Ba^{2+}$ occupying one-half of the octahedral holes, and $[Ga_2]$ dimers occupying the other half. In the other three structures, in turn, 3/4 of the octahedral holes are occupied by the cations, while the remaining quarter is occupied by $[Sn_2]$ or $[Si_2]$. In fact, a similar description has been given for $A_7Ga_8Sb_8$,[22] and can be extended to $EuIn_2Pn_2$,[6,43] $EuGa_2Pn_2$,[7] and $BaIn_2P_2$[8] structures as well. The different atomic arrangements for the latter and for $BaGa_2Pn_2$ ($Pn$ = P, As) can therefore be attributed not to the filling of the octahedral voids, but rather to the different ways the pnicogen octahedra share edges and the corresponding directions of the neighboring $[Ga_2]$ or $[In_2]$ dumbbells, making each of them unique structure types. In this sense, it is very clear that the cations also play an important role in determining the structure by affecting the packing efficiency of the anionic network. This will be discussed below in more detail in the context of the electronic structure.

**Electronic Structure.** TB-LMTO-ASA electronic band structure calculations were carried out for both $BaGa_2P_2$ and $BaGa_2As_2$. This was done to examine the electronic structure in detail, and to compare and contrast the chemical bonding. However, because of the similarity of the bonding characteristics, the plots of the density of states (DOS) and the crystal orbital Hamilton populations (COHP) are only shown for $BaGa_2As_2$. Total and partial DOS diagrams are displayed in Figure 3; COHP curves for selected interactions are shown in Figure 4. The DOS plots show a sizable (ca. 1 eV) band gap at the Fermi level, suggesting that the compound should be an intrinsic semiconductor. This, of course is to be expected, since $BaGa_2As_2$ is an electron-precise Zintl phase, as discussed already. However, this computational result could not be verified from resistivity measurements because traces of

(48) Eisenmann, B.; Jordan, H.; Schäfer, H. *Z. Anorg. Allg. Chem.* **1986**, *532*, 73–80.
(49) Eisenmann, B.; Schäfer, H. *Z. Anorg. Allg. Chem.* **1982**, *484*, 142–152.

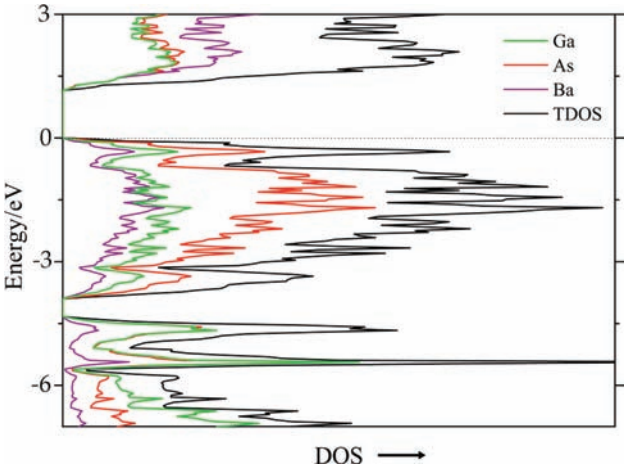


**Figure 3.** DOS diagrams for $BaGa_2As_2$. Total DOS is shown with a solid black line; partial DOS of Ba, Ga, and As are represented by purple, green, and red solid lines, respectively. $E_F$ (dotted line) is the energy reference at 0 eV.

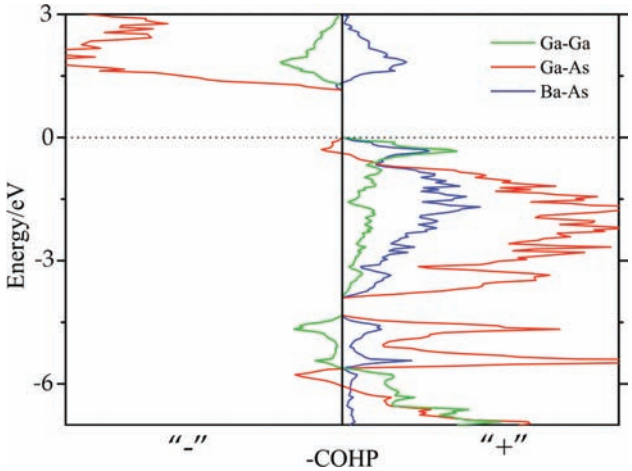


**Figure 4.** COHP curves for $BaGa_2As_2$. Contributions from Ba−As bonding are shown in blue, and the Ga−As and Ga−Ga interactions are shown in red and green, respectively. Since the "inverted" COHP values are plotted, the "+" regions represent the bonding interactions, while the "−" regions denote the states with antibonding character.

Ga flux caused the bulk material to appear metallic-like (despite the positive $d\rho/dT$, room temperature resistivity was large, and the residual resistivity at low temperature was also very high; see Supporting Information for details).

The states just below the Fermi level are predominately composed of As p orbitals, mixing with Ga p and Ba d orbitals. This is indicative of strong interactions between As and Ga, as well as Ba and As. At lower energy level, from about −4.7 to −7 eV, the states are dominated by Ga s and some As p contributions. Significant separation of s and p orbitals is seen for both Ga and As, with As s orbitals lying even lower (outside of the plotted region), in agreement with the higher electronegativity of As.[44] The band structure of $BaGa_2P_2$ is qualitatively the same, with the most noticeable differences being (1) a slightly wider energy gap; and (2) a slightly smaller separation of Ga and P valence states. In both cases, the substantial contribution of Ba 5d just below the Fermi level indicates that treating the $Ba^{2+}$ cations as electron donors and space filler is an oversimplification. Mixing of barium and pnicogen orbitals in the valence band signifies the significant covalency of the Ba−*Pn* bonding. Following this reasoning, it can be seen that the more ionic character of the Ba−P interactions compared with the Ba−As interactions is the primary cause for the widening of the band gap.

The COHP curves for the averaged Ga−As, Ga−Ga, and Ba−As interactions are projected in Figure 4. As seen from the plot, the Ga−Ga interactions are fully optimized at the Fermi level, suggesting a strong covalent bond and are consistent with the short bond distances. Ga−As bonding is nearly optimized, showing some antibonding character just below the Fermi level. Similar antibonding character of Ga−*Pn* bonds is also known for those compounds where strong homoatomic Ga−Ga bonding is present, for example, $BaGa_2Sb_2$,[1] $Ba_3Ga_4Sb_5$,[11] and $Eu_7Ga_6Sb_8$,[50] and could be attributed to the low oxidation state of Ga.[50] To the contrary, the Ba−As interactions retain some of their bonding character above the Fermi level, suggesting that further chemical reduction, that is, filling more electrons into these bands, may strengthen the Ba−As bonding. This effect, of course, will be counterbalanced by the destabilization of the Ga−As substructure. Nonetheless, although well balanced, the system appears to be able to withstand heavy *n*- or *p*-doping, which would alter the states closer to the Fermi level, thereby influencing the electronic transport properties.

(50) Park, S. M.; Kim, S. J.; Kanatzidis, M. G. *J. Solid State Chem.* **2004**, *177*, 2867–2874.

## Conclusions

Two new Zintl compounds, $BaGa_2P_2$ and $BaGa_2As_2$, have been synthesized from Ga-flux reactions and structurally characterized. They are isostructural and their structures feature $^2_\infty[Ga_2Pn_2]^{2-}$ layers made up of condensed $[Ga_2Pn_6]$ ethane-like moieties. The electron count for both compounds follows the Zintl rules, and is in agreement with electronic band structure calculations. The inclusion of metallic gallium in the single-crystals has impeded the magnetic susceptibility and resistivity measurements, suggesting that suitable methods for removing Ga or different synthetic routes need to be developed. The discovery of these new compounds adds to the scarce structural and thermochemical data available for the Ba−Ga−As and Ba−Ga−P ternary systems, and hints at the possibility that more phases are likely to be found, provided that systematic and careful syntheses are undertaken.

**Acknowledgment.** Svilen Bobev acknowledges financial support from the University of Delaware and the Petroleum Research Fund (ACS-PRF). We also thank Prof. R. Greene, Dr. Sh. R. Saha, and Prof. J.-P. Paglione (Department of Physics, University of Maryland) for the magnetic susceptibility measurement on $BaGa_2P_2$ and $BaGa_2As_2$ and for useful discussions. Work at UMD was supported by an AFOSR MURI Award.

**Supporting Information Available:** A combined X-ray crystallographic file in CIF format, along with details of the synthesis, plots of the crystal structure with anisotropic displacement parameters; schematic representation relating the $^2_\infty[Ga_2As_2]^{2-}$ layers in $BaGa_2As_2$ with the $^1_\infty[Si_2As_4]^{6-}$ chains, known for the $Sr_3Si_2As_4$ structure type; drawings of the $CaAl_2Si_2$, $ThCr_2Si_2$, $CaBe_2Ge_2$, $BaGa_2Sb_2$, $EuGa_2As_2$, $BaIn_2P_2$, and $EuIn_2As_2$ structures; plots of $\chi(T)$ and $\rho(T)$ with a short discussion of the observed properties. This material is available free of charge via the Internet at http://pubs.acs.org.